

Article

# Modification of Copper Benzene-1,3,5-tricarboxy Late (Cu-BTC) Composites with Multiwalled Carbon Nanotubes and Amino Groups for Enhanced CO<sub>2</sub>/CH<sub>4</sub> Selective Adsorption Performance and Water Stability

Weiwei Jian <sup>1,\*</sup>, Qiuyan Hai <sup>1</sup>, Adili Youlidaxi <sup>1</sup>, Tianqiang Liu <sup>1</sup>, Danzhu Ma <sup>1,\*</sup> and Fengrui Jia <sup>2</sup>

<sup>1</sup> College of Petroleum Engineering, Liaoning Petrochemical University, Fushun 113000, China; yan632426864@hotmail.com (Q.H.); a891415033@hotmail.com (A.Y.); ltq990711@hotmail.com (T.L.)

<sup>2</sup> Yantze Delta Region Institute, Tsinghua University-Zhejiang, Jiaxing 314000, China; jiafengrui@tsinghua-zj.edu.cn

\* Correspondence: jianweiwei88@lnpu.edu.cn (W.J.); madanzhu@lnpu.edu.cn (D.M.)

**Abstract:** CNT-NH<sub>2</sub>-Cu-BTC was prepared via hydrothermal synthesis for the adsorption and separation of CO<sub>2</sub>/CH<sub>4</sub> mixtures with 2, 6, and 10% multiwalled carbon nanotube (MWCNT) additions. NH<sub>2</sub>-BTC composites were synthesized by changing the organic ligand and adding NH<sub>2</sub>-BDC (15, 25, 35, and 45%) to improve the adsorption capacity. MWCNTs were loaded to enhance the water stability of the material. The structure, surface morphology, and pore size distribution of the composites were characterized using X-ray diffraction, scanning electron microscopy, Fourier transform infrared spectroscopy, thermogravimetric analysis, and specific surface area and pore structure measurements. The CO<sub>2</sub>/CH<sub>4</sub> selective adsorption performance was studied via breakthrough experiments using a self-made adsorption device. The CO<sub>2</sub> adsorption capacity of Cu-BTC increased due to the addition of NH<sub>2</sub>-BDC, with 35%NH<sub>2</sub>-Cu-BTC exhibiting the best CO<sub>2</sub> adsorption property, i.e., a CO<sub>2</sub> adsorption capacity of 1.82 mmol/g and a CO<sub>2</sub>/CH<sub>4</sub> separation coefficient of 1.44 at 35 °C and 20 mL/min. After adding MWCNTs, 6%CNT-NH<sub>2</sub>-Cu-BTC exhibited the best CO<sub>2</sub> adsorption property and water stability, with the CO<sub>2</sub> adsorption capacity increasing to 2.06 mmol/g. 6%CNT-NH<sub>2</sub>-Cu-BTC with wet impregnation retained 79% of the CO<sub>2</sub> adsorption capacity of the sample without wet impregnation, demonstrating its excellent water stability under humid conditions. Cyclic experiments with and without wet impregnation were performed.

**Keywords:** CO<sub>2</sub>/CH<sub>4</sub> separation; CNT-NH<sub>2</sub>-Cu-BTC; water stability



**Citation:** Jian, W.; Hai, Q.; Youlidaxi, A.; Liu, T.; Ma, D.; Jia, F. Modification of Copper Benzene-1,3,5-tricarboxy Late (Cu-BTC) Composites with Multiwalled Carbon Nanotubes and Amino Groups for Enhanced CO<sub>2</sub>/CH<sub>4</sub> Selective Adsorption Performance and Water Stability. *Processes* **2024**, *12*, 745. <https://doi.org/10.3390/pr12040745>

*Processes* **2024**, *12*, 745. <https://doi.org/10.3390/pr12040745>

Academic Editor: Federica Raganati

Received: 13 March 2024

Revised: 3 April 2024

Accepted: 3 April 2024

Published: 7 April 2024



**Copyright:** © 2024 by the authors. Licensee MDPI, Basel, Switzerland. This article is an open access article distributed under the terms and conditions of the Creative Commons Attribution (CC BY) license (<https://creativecommons.org/licenses/by/4.0/>).

## 1. Introduction

Heat release associated with the combustion of methane (CH<sub>4</sub>), which is the main component of biogas and natural gas, can reach 34,000 KJ/m<sup>3</sup> per unit volume. However, biogas, in which CH<sub>4</sub> and carbon dioxide (CO<sub>2</sub>) account for 55–70% and 25–40%, respectively [1], and natural gas contain a large amount of CO<sub>2</sub> gas [2], which affects fuel utilization and reduces the calorific value of fuel combustion. Therefore, separation of CO<sub>2</sub> from fuel is essential to achieve carbon emission reduction and effective energy utilization, and adsorption stands out as a promising method for this purpose [3,4]. Wang et al. [5] used Ca(Ac)<sub>2</sub> as a precursor to modified CaO, and a favorable adsorption property was found for CO<sub>2</sub> adsorption. In the case of water vapor diffusion, the adsorbent also showed excellent CO<sub>2</sub> adsorption performance, and the adsorption capacity remained above 65% after 18 cycles. Cláudio et al. [6] prepared hydrotalc (HTCs) to evaluate the CO<sub>2</sub> adsorption capacity of HTCs. The CO<sub>2</sub> adsorption capacity was 1.05 mmol/g at a pressure of 1 bar and a temperature of 300 °C.

Selecting an appropriate adsorbent is critical for the adsorption separation of CO<sub>2</sub> and CH<sub>4</sub> [7]. At present, solid adsorbents are widely used in the field of gas adsorption [8].

Specifically, metal–organic framework (MOF) materials are popular as solid adsorbents because of their variable structure and easy modification. Additionally, MOF materials have a high specific surface area, flexible frame, and unsaturated metal sites, which are beneficial for adsorption. Various MOFs have been used for CO<sub>2</sub> adsorption [9–12], such as UiO-66, ZIF-8, and Cu-BTC, among which Cu-BTC has attracted increasing attention recently owing to its high chemical stability, simple preparation, easy availability, and inexpensive precursors. However, the adsorption capacity, separation coefficient, and water stability of Cu-BTC at atmospheric pressure are still not satisfactory. Therefore, improving the selective adsorption and water stability of Cu-BTC materials is necessary for practical applications.

Recent research aiming to improve the CO<sub>2</sub> adsorption capacity of Cu-BTC and the selective adsorption of CO<sub>2</sub> in the mixed gas has focused on the modification of Cu-BTC. The affinity of alkali amines for acidic CO<sub>2</sub> is well known; therefore, functionalization of the open metal sites in Cu-BTC with various amines provides a promising approach to improve the CO<sub>2</sub> capture performance. The addition of polyamides and diamines to the MOF backbone can considerably improve the CO<sub>2</sub> adsorption capacity at room temperature and low pressure. For example, Salehi et al. [13] studied the adsorption capacity and selectivity of amino-modified Cu-BTC and MOF/NPC adsorbents for CO<sub>2</sub>, CH<sub>4</sub>, and N<sub>2</sub>. Compared with MOF/NPC, which captures CO<sub>2</sub> via physical adsorption, amine-modified MOF/NPC operates via chemical adsorption, which favors the adsorption of CO<sub>2</sub> over that of CH<sub>4</sub> and N<sub>2</sub>, improving markedly the selectivity of the material for CO<sub>2</sub>. Additionally, carbon-based materials have been combined with Cu-BTC to improve the CO<sub>2</sub> adsorption performance of MOF materials. Ullah et al. [14] successfully synthesized (MWCNT)@Cu-BTC composites, finding that the CO<sub>2</sub> adsorption capacity of Cu-BTC and MWCNT@Cu-BTC increased from 1.92 to 3.26 mmol/g, possibly due to the generation of new pore structures via the interaction between MWCNTs and Cu-BTC crystals.

Zhang et al. [15] synthesized Cu-BTC, Mg/Cu-BTC, Cu-BTC@MWCNT, and Mg/Cu-BTC@MWCNT as CO<sub>2</sub> adsorbents. The results show that Mg<sup>2+</sup>- and MWCNT-doped Cu-BTC can affect the physical properties of the adsorbent. Under the conditions of 25 °C and 100 kPa, Mg/Cu-BTC@MWCNT exhibited the best CO<sub>2</sub> adsorption capacity (3.63 mmol/g) and selectivity (14.28 mmol/g). Eshraghi et al. [16] prepared CNT@MIL-100 and CNT@Cu<sub>3</sub>(BTC)<sub>2</sub> to research CO<sub>2</sub> adsorption. The CO<sub>2</sub> adsorption capacity of CNT@MIL-100 and CNT@Cu<sub>3</sub>(BTC)<sub>2</sub> was significantly increased compared to Cu-BTC at 298 K. The addition of MWCNTs increased the volume of micropores, which may be the reason for the increase in CO<sub>2</sub> adsorption capacity. Xiang et al. [17] prepared CNT@Cu<sub>3</sub>(BTC)<sub>2</sub> and investigated the selectivity of the equivalent molar CO<sub>2</sub>/CH<sub>4</sub> mixture. The selectivity is between 5.5 and 7.0, which is higher than that of activated carbon.

The organic ligands of Cu-BTC can be easily replaced by water molecules in humid environments, resulting in the collapse of the skeleton structure. At present, common methods to improve the water stability of MOF materials mainly include the modification of hydrophobic groups in the ligands [18], using inert metal clusters, or covering the crystal surface with hydrophobic layers. Li et al. [19] proposed a new method to improve the water stability of Cu-BTC, which involved the functionalization of Cu-BTC with imidazole to obtain Imi@Cu-BTC. Compared with Cu-BTC, the water stability of Imi@Cu-BTC was substantially improved. When Cu-BTC was exposed to humid air for 20 days, it lost nearly all its crystallinity and retained only 6% of its original CO<sub>2</sub> adsorption capacity, whereas Imi1/3@Cu-BTC successfully retained its main crystal structure and 78% of its initial CO<sub>2</sub> adsorption capacity. The CO<sub>2</sub> adsorption capacity of Imi@Cu-BTC was 4.4 mmol/g at atmospheric pressure and room temperature, which is much higher than that of ZIF-8, UiO-66, and MIL-101. Meanwhile, Yu et al. [20] successfully synthesized a novel hydrophobic adsorbent, Cu-BTC-(n)Br, using Cu(NO<sub>3</sub>)<sub>2</sub> and BTC-(n)Br as precursors. Compared with untreated Cu-BTC, Cu-BTC-(n)Br showed obvious hydrophobicity and adsorption effects in a water environment.

These investigations proved that Cu-BTC and its modified materials can effectively improve the CO<sub>2</sub> adsorption capacity or the water stability of MOFs, but only a few studies have considered both effects simultaneously. Herein, the preparation of NH<sub>2</sub>-Cu-BTC and CNT-NH<sub>2</sub>-Cu-BTC composites, which can simultaneously improve the CO<sub>2</sub>/CH<sub>4</sub> selective adsorption performance and water stability, is described. The prepared composites were characterized via X-ray diffraction (XRD) were supplied by Bruker (Billerica, MA, USA), scanning electron microscopy (SEM) were supplied by Hitachi (Tokyo, Japan), Fourier transform infrared (FT-IR) spectroscopy were supplied by Bruker (Billerica, MA, USA), thermogravimetric analysis (TGA) were supplied by NETZSCH (Selb, Germany), and Brunauer–Emmett–Teller (BET) specific surface area and pore structure measurements were supplied by Conta (Punta Gorda, FL, USA). CO<sub>2</sub>/CH<sub>4</sub> selective adsorption measurements were performed using a self-made adsorption apparatus. The influence of temperature, flow rate, and recycling on adsorption is also discussed. Furthermore, the water stability of different samples was evaluated by exposing them to a water environment for 12 h.

## 2. Materials and Methods

### 2.1. Materials

Copper nitrate trihydrate (99.0%), benzene-1,3,5-tricarboxylic acid (H<sub>3</sub>BTC, 98.0%), and *N,N*-dimethylformamide (DMF, 99.9%) were purchased from Maclean Biochemical Technology Co., Ltd. (Shanghai, China). Absolute ethanol (99.7%) was purchased from Sinopharm Chemical Reagent Co., Ltd. (Beijing, China). 2-Aminoterephthalic acid (98.0%) was purchased from Thermo Fisher Scientific Co., Ltd. (Waltham, MA, USA). MWCNTs (95%) were purchased from Chengdu Organic Chemical Co., Ltd., Chinese Academy of Sciences (Chengdu, China). Concentrated sulfuric acid (98%) and concentrated nitric acid (68%) were purchased from Nanjing Chemical Pharmaceutical Co., Ltd. (Nanjing, China). The deionized water used for washing and preparing the solutions was prepared in the laboratory.

### 2.2. Preparation of Cu-BTC

Cu-BTC was prepared as follows [21]: first, Cu(NO<sub>3</sub>)<sub>2</sub>·3H<sub>2</sub>O (2.5 g) and H<sub>3</sub>BTC (1.25 g) were added to a solution containing absolute ethanol/DMF in a molar ratio of 2:1. The mixture was sonicated repeatedly for 30 min and stirred for 1 h until a homogeneous solution was obtained. Next, the homogeneous solution was poured into a hydrothermal reactor and dried at 100 °C in a blast drying oven for 48 h. The sample was removed, cooled to room temperature, and washed three times using a mixture of anhydrous ethanol and deionized water to remove unreacted ions and impurities. The solid product was recovered via filtration and dried in a vacuum oven at 120 °C for 24 h to obtain the Cu-BTC material. The as-prepared Cu-BTC material was ground into powder and sealed for storage. Before each use, reactivation in a vacuum oven for 5 h was performed to remove guest molecules.

### 2.3. Preparation of NH<sub>2</sub>-Cu-BTC

Four different NH<sub>2</sub>-Cu-BTC samples were prepared, i.e., 15%NH<sub>2</sub>-Cu-BTC, 25%NH<sub>2</sub>-Cu-BTC, 35%NH<sub>2</sub>-Cu-BTC, and 45%NH<sub>2</sub>-Cu-BTC, using a similar procedure to that of Cu-BTC except that a certain amount 2-aminoterephthalic acid (15%, 25%, 35%, and 45% relative to H<sub>3</sub>BTC, respectively) was added to the mixture of absolute ethanol and DMF.

### 2.4. Preparation of CNT-NH<sub>2</sub>-Cu-BTC

Before loading into NH<sub>2</sub>-Cu-BTC, MWCNTs were impregnated in a mixture of sulfuric acid and nitric acid at a mole ratio of 3:1 at 50 °C for 24 h while stirring. The suspension liquid was then washed with deionized water until neutral. Finally, the acidified MWCNTs were dried at 60 °C for 24 h and collected for subsequent use.

Three different composite adsorbents, i.e., 2%CNT-NH<sub>2</sub>-Cu-BTC, 6%CNT-NH<sub>2</sub>-Cu-BTC, and 10%CNT-NH<sub>2</sub>-Cu-BTC, were prepared with MWCNT mass fractions of 2%, 6%, and 10%, respectively. The preparation of 2%CNT-NH<sub>2</sub>-Cu-BTC is described as an example.

Here, 2 wt.% (mass percentage of NH<sub>2</sub>-Cu-BTC expected yield) of acidified MWCNTs was placed in a mixed solution of NH<sub>2</sub>-BDC, H<sub>3</sub>BTC, and Cu(NO<sub>3</sub>)<sub>2</sub>, fully dissolved, and dried in a blast drying oven at 100 °C for 48 h. Subsequently, the samples were washed with a mixture of deionized water and ethanol three times, filtered, and placed in a vacuum-drying oven for 24 h to obtain the composite materials. The as-prepared samples were packed in sealed bags after grinding into powder and reactivated in a vacuum-drying oven for 5 h before each use.

### 2.5. Wet Treatment

The prepared samples were impregnated in an equal volume of deionized water for 12 h. After impregnation, the samples were filtered and heated at 200 °C for 6 h in a blast drying oven at a heating rate of 5 °C/min.

### 2.6. Desorption of CNT-NH<sub>2</sub>-BTC Composites in Cyclic Experiments

The recycling performance of adsorbents is an important index for evaluating their performance. After each adsorption experiment, the sample was placed in a vacuum drying oven and vacuum heated at 100 °C for 5 h to degas. Subsequently, they were subjected to cyclic experiments.

### 2.7. Characterization

XRD (D8Advance, made by Bruker, Billerica, MA, USA) with Cu K $\alpha$  radiation operated at 40 kV and 40 mA was used to determine the crystal structure. The scanning range was 5–90° and the scanning speed was 0.02°/s. SEM (SU8010 made by Hitachi, Tokyo, Japan) was used to observe the surface morphology of the samples, which were sprayed with gold before scanning. FT-IR spectroscopy (EQUINOX-55, Bruker) in the wavenumber range of 500–4000 cm<sup>-1</sup> was used to determine the functional groups. To eliminate the influence of moisture on the analysis results, all samples were dried at 120 °C for 4 h before testing. To determine the specific surface area and pore volume of the material, BET N<sub>2</sub> adsorption–desorption isotherms were obtained (Autosorb-IQ2-MP, made by Cantata, FL, USA). All samples were degassed at 100 °C for 8 h before testing. The specific surface area of the samples was calculated using the BET equation, and the pore volume and pore size distribution were determined on the basis of the amount of adsorbed N<sub>2</sub>. Furthermore, TGA (STA449C, NETZSCH GmbH) was used to evaluate the thermal stability of the prepared composites.

### 2.8. CO<sub>2</sub> and CH<sub>4</sub> Adsorption Experiments

The adsorption experiments were conducted using a self-made adsorption apparatus comprising a gas supply system, a fixed-bed adsorber, and a data acquisition system (Figure 1). A 4.48VOL%:25.52 VOL% CO<sub>2</sub>/CH<sub>4</sub> mixture was supplied by a gas cylinder. First, the adsorbent was placed on the fixed bed at the experimental temperature; second, N<sub>2</sub> was injected to purify the experimental system; third, the flow rate of the mixed gas cylinder was adjusted to the experimental value, and the data were recorded in real-time until the end of the experiment; finally, the next temperature and flow rate were adjusted and the above steps were repeated. To ensure the accuracy of the experimental results, the experiments were repeated three times, and average values were considered.

The following formula was used to calculate the adsorption capacity:

$$Q = \frac{\int_0^t L(C_0 - C)dt}{22.4 * m} \quad (1)$$

Here,  $Q$  is the adsorption capacity (mmol/g),  $t$  is the time (s),  $L$  is the total gas flow rate (mL/min),  $C_0$  is the initial concentration of CO<sub>2</sub> or CH<sub>4</sub> (vol.%),  $C$  is the outlet concentration of CO<sub>2</sub> or CH<sub>4</sub> (vol.%), and  $m$  is the adsorbent mass (g).

To evaluate the adsorption selectivity of the adsorbent, the  $\text{CO}_2$  separation coefficient was obtained as follows:

$$S = \frac{Q_1/p_1}{Q_2/p_2} \quad (2)$$

Here,  $S$  is the  $\text{CO}_2$  separation coefficient,  $Q_1$  is the  $\text{CO}_2$  adsorption capacity (mmol/g),  $Q_2$  is the  $\text{CH}_4$  adsorption capacity (mmol/g), and  $p_1$  and  $p_2$  are the partial pressures of  $\text{CO}_2$  and  $\text{CH}_4$  in the gas mixture, respectively.

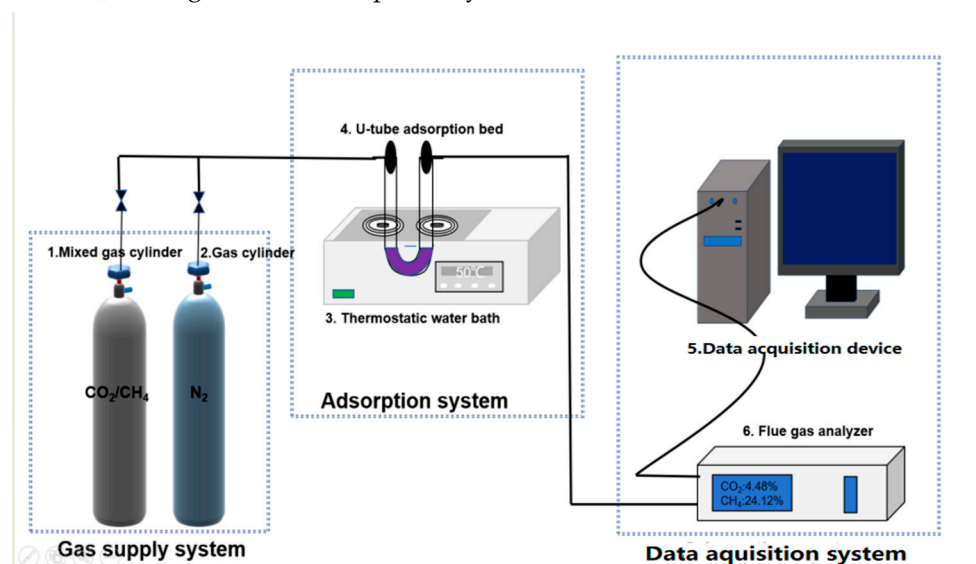


Figure 1. Schematic of the setup for the adsorption experiments.

### 3. Results and Discussion

#### 3.1. Adsorbent Characterization

Crystal structures of the composites were characterized via XRD. Figure 2 illustrates the XRD patterns of Cu-BTC, 35% $\text{NH}_2$ -Cu-BTC, and 6% $\text{CNT-NH}_2$ -Cu-BTC.

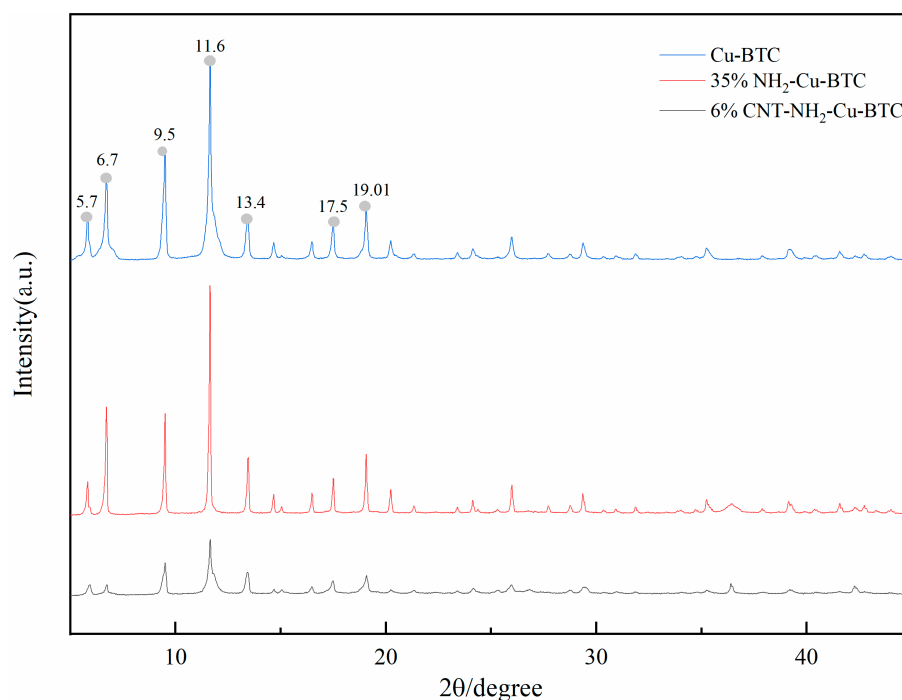
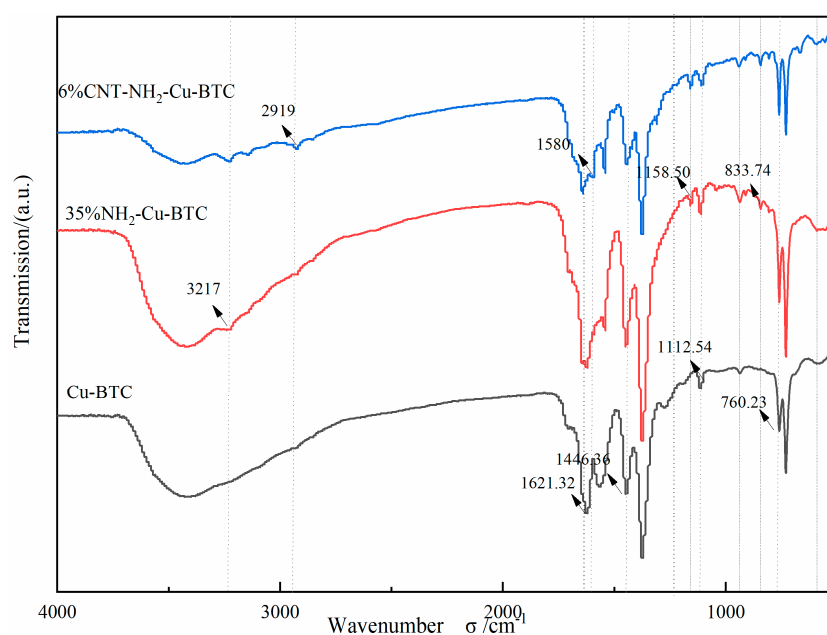


Figure 2. X-ray diffraction patterns of Cu-BTC, 35% $\text{NH}_2$ -Cu-BTC, and 6% $\text{CNT-NH}_2$ -Cu-BTC.

The characteristic peaks of Cu-BTC were observed at  $2\theta$  values of  $5.7^\circ$ ,  $6.7^\circ$ ,  $9.5^\circ$ ,  $11.6^\circ$ ,  $13.4^\circ$ ,  $17.5^\circ$ , and  $19.01^\circ$ , which are consistent with those previously reported [12]. The XRD patterns of 35%NH<sub>2</sub>-Cu-BTC and 6%CNT-NH<sub>2</sub>-Cu-BTC showed similar peaks to those of Cu-BTC, indicating that the crystal structure was well preserved during the synthesis process. No significant MWCNT peak was observed due to the low incorporation ratio of MWCNTs. The intensities of the characteristic peaks for 35%NH<sub>2</sub>-Cu-BTC and 6%CNT-NH<sub>2</sub>-Cu-BTC were slightly lower than that of Cu-BTC, which may be ascribed to the strong binding of the added amines and MWCNTs to Cu-BTC.

Furthermore, FT-IR spectroscopy was used to determine whether the functional groups were successfully loaded onto Cu-BTC. The FT-IR spectra of Cu-BTC, 35%NH<sub>2</sub>-Cu-BTC, and 6%CNT-NH<sub>2</sub>-Cu-BTC are depicted in Figure 3.



**Figure 3.** Fourier transform infrared spectra of Cu-BTC, 35%NH<sub>2</sub>-Cu-BTC, and 6%CNT-NH<sub>2</sub>-Cu-BTC.

The complete vibrational spectrum of Cu-BTC was in agreement with published data [22]. In the spectrum of pristine Cu-BTC, the peaks at  $1621.32$  and  $1446.36$   $\text{cm}^{-1}$  correspond to the C–C skeletal vibration of the benzene groups in the BTC linker and the asymmetric COO stretching, respectively. The peak at  $1112.54$   $\text{cm}^{-1}$  corresponds to C–O–Cu stretching, and the band around  $760.23$   $\text{cm}^{-1}$  represents the Cu substitution on the benzene groups. The peak at  $1158.50$   $\text{cm}^{-1}$  corresponds to the stretching of the C–N bond, and the new peaks at  $3217$   $\text{cm}^{-1}$  and  $833.74$   $\text{cm}^{-1}$  belong to N–H, further proving the presence of amino groups in NH<sub>2</sub>-Cu-BTC. A characteristic peak appearing at  $1580$   $\text{cm}^{-1}$  can be attributed to the vibration of the carbon skeleton in the MWCNTs [23], and the new peak at  $2919$   $\text{cm}^{-1}$  is caused by -OH expansion in -COOH.

SEM analysis was used to study the surface topography of the samples, as depicted in Figure 4.

Figure 4a,b shows that Cu-BTC exhibits an octahedral structure, as previously reported [13]. When Cu-BTC was impregnated with an equal volume of deionized water for 12 h, the octahedral structure collapsed and Cu-BTC material degraded into a layered structure, as shown in Figure 4c,d, indicating that the water stability of Cu-BTC was poor. As shown in Figure 4e,f, some roughness appeared on the surface of Cu-BTC, modified by the NH<sub>2</sub>-BDC functional groups. The NH<sub>2</sub>-BDC modification did not improve the water stability of Cu-BTC, and NH<sub>2</sub>-Cu-BTC still collapsed into a layered structure after impregnation Figure 4g,h. When an appropriate amount of MWCNTs was added, uneven particles were

attached to the crystal surface Figure 4i,j. After wet impregnation (Figure 4k,l), 6%CNT-NH<sub>2</sub>-Cu-BTC maintained the original Cu-BTC crystal structure, which indicated that the addition of MWCNTs effectively improved the water stability of the material.

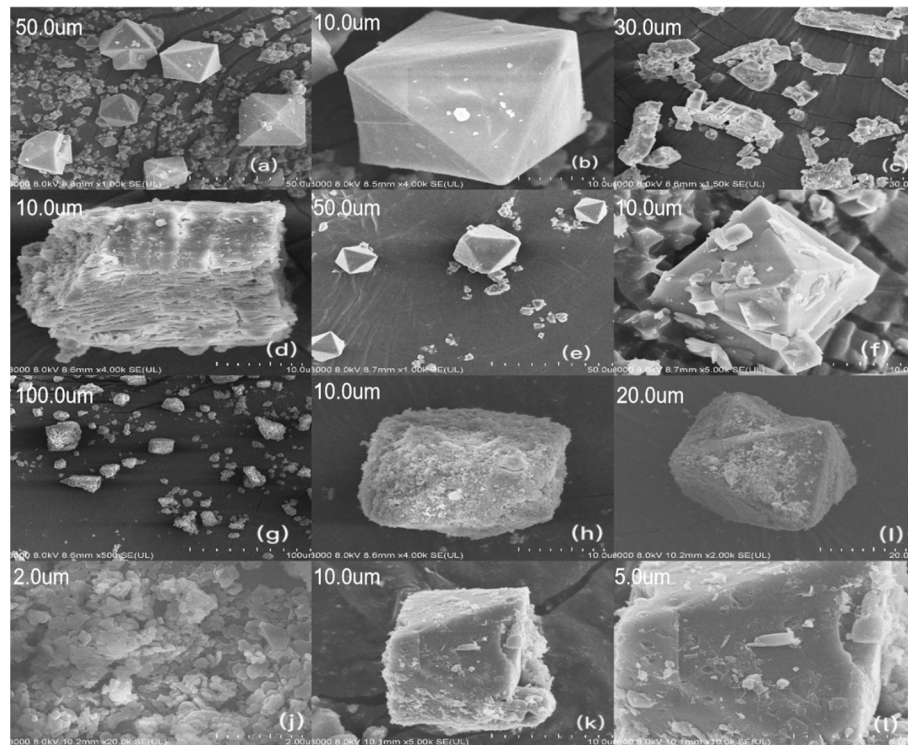


**Figure 4.** Scanning electron microscopy images of (a,b) Cu-BTC, (c,d) Cu-BTC (wet), (e,f) 35%NH<sub>2</sub>-Cu-BTC, (g,h) 35%NH<sub>2</sub>-Cu-BTC (wet), (i,j) 6%CNT-NH<sub>2</sub>-Cu-BTC, and (k,l) 6%CNT-NH<sub>2</sub>-Cu-BTC (wet).

The N<sub>2</sub> adsorption–desorption isotherms of different samples were determined at 77 K, as shown in Figure 5.

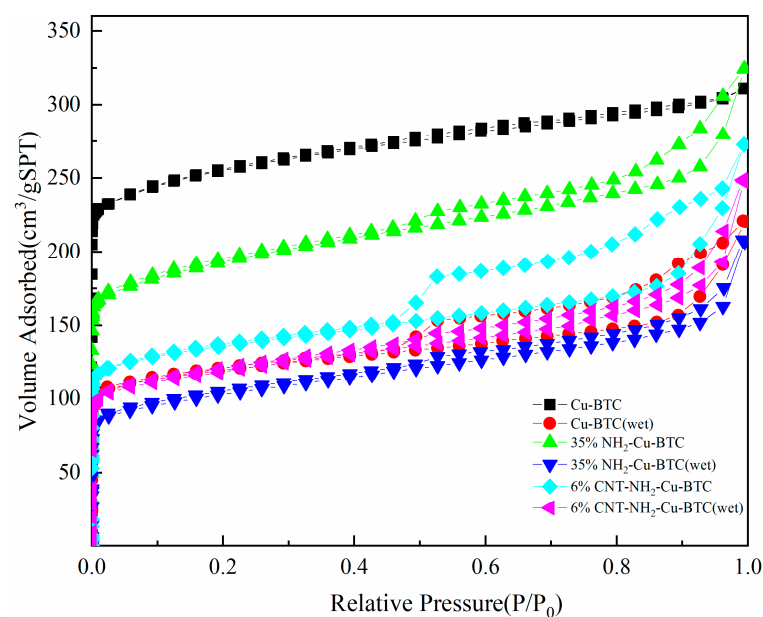


**Figure 5.** N<sub>2</sub> adsorption–desorption isotherms at 77 K on Cu-BTC, Cu-BTC (wet), 35%NH<sub>2</sub>-Cu-BTC, 35%NH<sub>2</sub>-Cu-BTC (wet), 6%CNT-NH<sub>2</sub>-Cu-BTC, and 6%CNT-NH<sub>2</sub>-Cu-BTC (wet) samples.

As can be seen in Figure 5, the adsorption curves correspond to typical I-type isotherms, which are indicative of a microporous structure. This was confirmed by the pore size distributions depicted in Figure 6. The pore volume of 6%CNT-NH<sub>2</sub>-Cu-BTC is smaller than that of both 35% NH<sub>2</sub>-Cu-BTC and Cu-BTC. The crystallinity of 6%CNT-NH<sub>2</sub>-Cu-BTC in the XRD image (Figure 2) decreased after the addition of carbon nanotubes, which may be the reason for the decrease in the pore volume of 6%CNT-NH<sub>2</sub>-Cu-BTC.

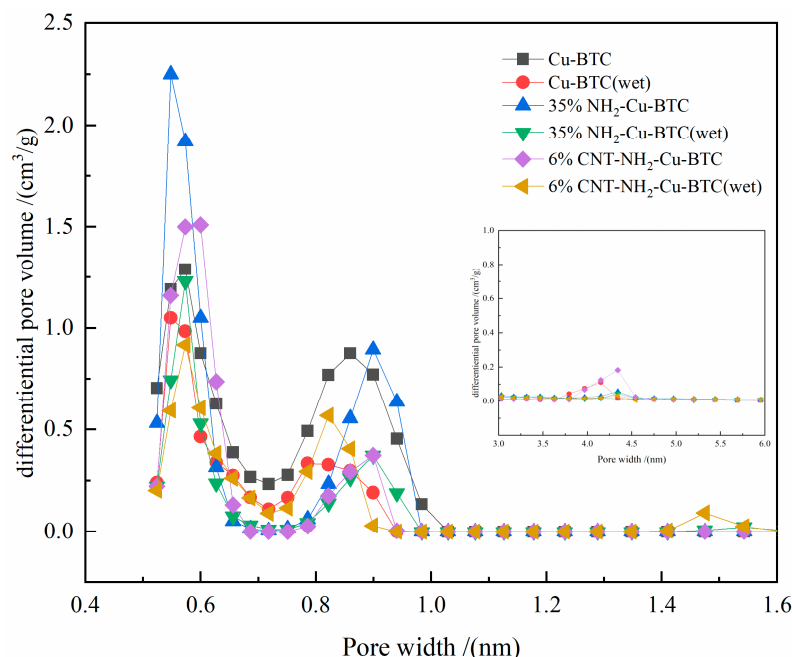


**Figure 6.** Pore size distribution curves of Cu-BTC, Cu-BTC (wet), 35%NH<sub>2</sub>-Cu-BTC, 35%NH<sub>2</sub>-Cu-BTC (wet), 6%CNT-NH<sub>2</sub>-Cu-BTC, and 6%CNT-NH<sub>2</sub>-Cu-BTC (wet).

Moreover, an H4-type obvious hysteresis loop was observed in the adsorption curve of 6%CNT-NH<sub>2</sub>-Cu-BTC, indicating that the material contained a mixture of micropores and mesopores after the addition of MWCNT. The hysteresis loop also indicates the occurrence of different interaction forces between N<sub>2</sub> molecules and the solid surface during adsorption and desorption. The mesopores of 6%CNT-NH<sub>2</sub>-Cu-BTC are shown in Figure 6, with pore widths ranging from 4 to 4.5 nm.

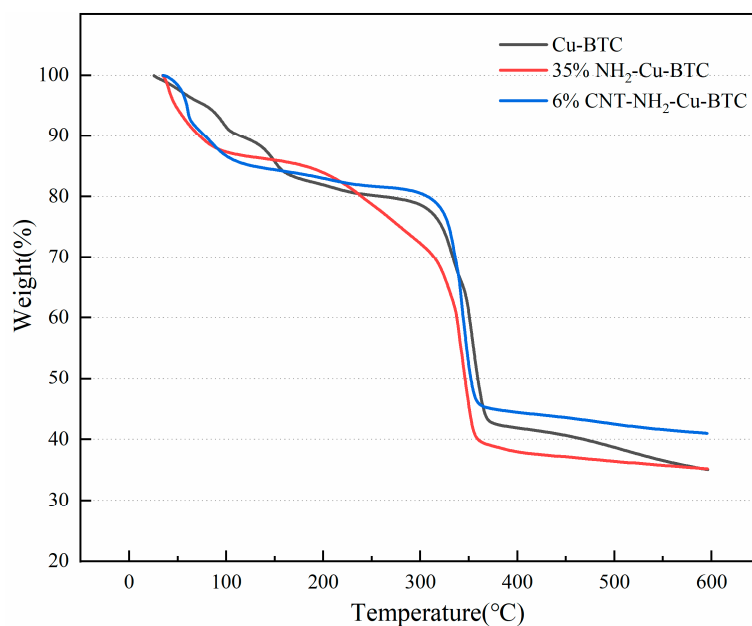
As depicted in Figure 6, the BJH method was applied to determine the pore size distribution and revealed that the samples were concentrated at 0.5–0.7 nm, which is characteristic of an extremely microporous structure conducive to the adsorption and storage of small gas molecules such as CO<sub>2</sub>.

The textural properties of different samples are reported in Table 1. The BET surface areas and pore volumes decreased after modification. The reason may be that the introduction of –NH<sub>2</sub> and MWCNTs blocks the pores of Cu-BTC. The BET surface area and pore volume of the samples decreased after wet impregnation, with 6%CNT-NH<sub>2</sub>-Cu-BTC showing the lowest absolute and relative decreases. The relative decreases in the BET surface and pore volume for 6%CNT-NH<sub>2</sub>-Cu-BTC were 14% and 10%, respectively. This indicates that the framework structure of Cu-BTC is destroyed by wet impregnation, but the addition of MWCNTs is conducive to maintaining the framework structure, most likely due to the hydrophobicity of MWCNTs protecting the composite from wet impregnation. These results are consistent with the SEM results.

**Table 1.** Textural properties determined by N<sub>2</sub> adsorption–desorption experiments at 77 K.

Sample	BET Surface Area (m <sup>2</sup> /g)	Relative Reduction in the BET Surface Area	Pore Volume (cm <sup>3</sup> /g)	Relative Reduction in Pore Volume
Cu-BTC	990.6	--	0.48	--
Cu-BTC (wet)	454.1	54%	0.34	29%
35%NH <sub>2</sub> -Cu-BTC	726.6	--	0.50	--
35%NH <sub>2</sub> -Cu-BTC (wet)	379.0	48%	0.32	36%
6%CNT-NH <sub>2</sub> -Cu-BTC	515.2	--	0.42	--
6%CNT-NH <sub>2</sub> -Cu-BTC (wet)	444.6	14%	0.38	10%

TGA was used to test the thermal stability of Cu-BTC, 35%NH<sub>2</sub>-Cu-BTC, and 6%CNT-NH<sub>2</sub>-Cu-BTC, as shown in Figure 7. For all samples, weight loss occurred mainly in two stages, i.e., a first stage occurring at 110 °C due to the release of guest molecules such as water molecules, and a second stage in the temperature range from 300 °C to 350 °C caused by the collapse of the material skeleton. In the range of 100–300 °C, 6%CNT-Cu-BTC, and Cu-BTC reached a plateau and then declined slowly, and the NH<sub>2</sub>-Cu-BTC sample has a significant weight loss of between 200 and 300 °C.

**Figure 7.** Thermogravimetric analysis of Cu-BTC, 35%NH<sub>2</sub>-Cu-BTC, and 6%CNT-NH<sub>2</sub>-Cu-BTC.

### 3.2. Adsorption of CO<sub>2</sub>/CH<sub>4</sub> Mixtures and Selectivity

#### 3.2.1. CO<sub>2</sub> Adsorption Capacity and CO<sub>2</sub>/CH<sub>4</sub> Selective Adsorption of NH<sub>2</sub>-Cu-BTC and CNT-NH<sub>2</sub>-Cu-BTC

##### (1) Effect of NH<sub>2</sub>-BDC addition on the CO<sub>2</sub>/CH<sub>4</sub> selective adsorption of NH<sub>2</sub>-Cu-BTC

The breakthrough curves of NH<sub>2</sub>-Cu-BTC with different NH<sub>2</sub>-BDC additions (0, 15, 25, 35, and 45%) are shown in Figure 8. The experiments were conducted at 35 °C and 20 mL/min. With increasing NH<sub>2</sub>-BDC addition, the CO<sub>2</sub> breakthrough time first increased and then decreased. Notably, 35%NH<sub>2</sub>-Cu-BTC exhibited the longest breakthrough time (28 min), whereas CO<sub>2</sub> breakthrough occurred at the beginning of the adsorption for 45%NH<sub>2</sub>-Cu-BTC. The CO<sub>2</sub> adsorption capacities of NH<sub>2</sub>-Cu-BTC with different NH<sub>2</sub>-BDC additions are shown in Figure 9. The CO<sub>2</sub> adsorption capacity of 35%NH<sub>2</sub>-Cu-BTC was the highest (1.82 mmol/g), whereas only 0.55 mmol/g CO<sub>2</sub> was absorbed by 45%NH<sub>2</sub>-Cu-BTC. These results are consistent with those shown in Figure 8. The NH<sub>2</sub>-BDC chains play a key role during the CO<sub>2</sub> adsorption process. Specifically, the amino groups react

with CO<sub>2</sub> to form methyl carbamate, promoting the CO<sub>2</sub> adsorption on NH<sub>2</sub>-Cu-BTC. However, excessive addition of NH<sub>2</sub>-BDC may occupy the original adsorption sites of Cu-BTC, thereby affecting its adsorption effectiveness, thus inhibiting the CO<sub>2</sub> adsorption. In this study, an NH<sub>2</sub>-BDC addition of 35% provided the best results, compared with the parent material Cu-BTC, the adsorption capacity increased by 1.51 mmol/g. Moreover, all the samples showed favorable CO<sub>2</sub>/CH<sub>4</sub> selective adsorption properties because the separation coefficients were all greater than one.

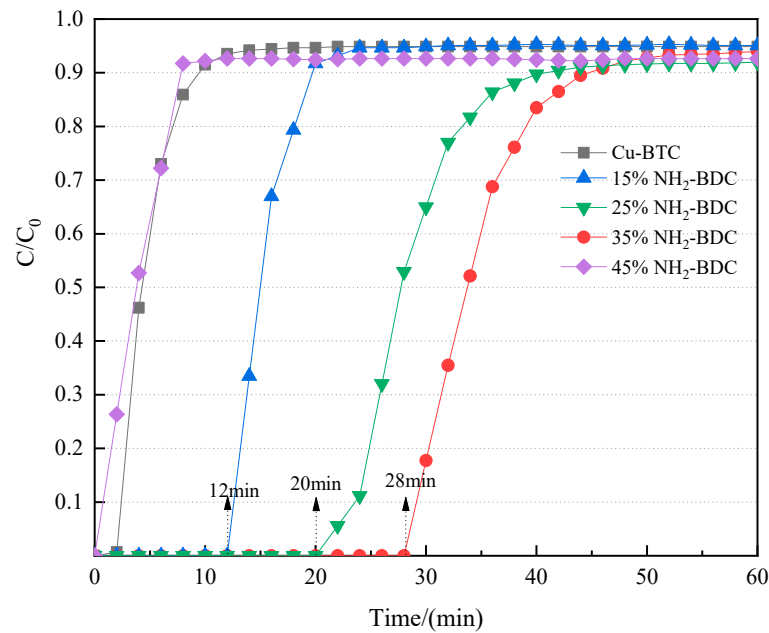


**Figure 8.** CO<sub>2</sub> breakthrough curves of NH<sub>2</sub>-Cu-BTC with different NH<sub>2</sub>-BDC additions.

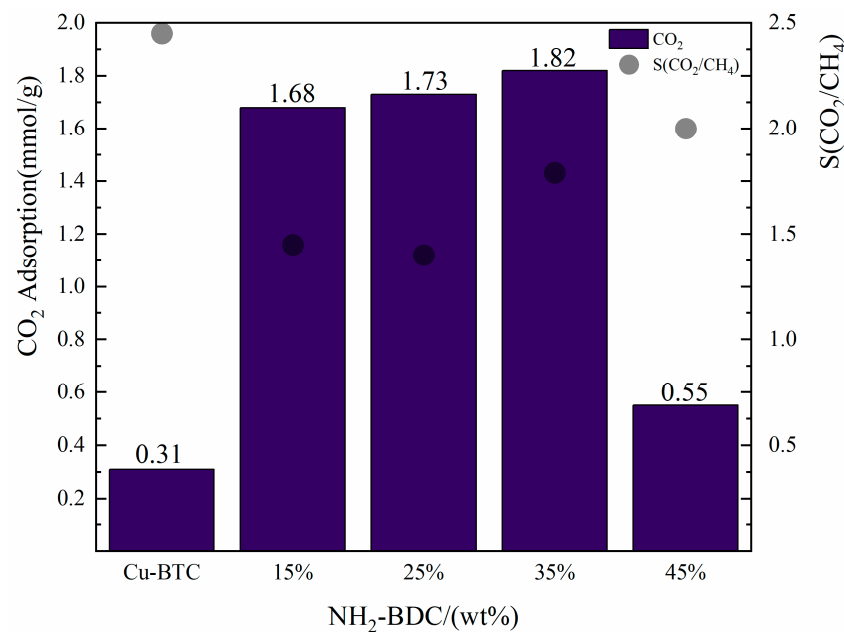


**Figure 9.** CO<sub>2</sub> adsorption capacity and selectivity of NH<sub>2</sub>-Cu-BTC with different NH<sub>2</sub>-BDC additions.

(2) Effect of MWCNT loading on the CO<sub>2</sub>/CH<sub>4</sub> selective adsorption of CNT-NH<sub>2</sub>-Cu-BTC

To evaluate the effect of the MWCNT loading on the CO<sub>2</sub>/CH<sub>4</sub> selective adsorption of CNT-NH<sub>2</sub>-Cu-BTC, experiments were performed using 35%NH<sub>2</sub>-Cu-BTC and CNT-NH<sub>2</sub>-Cu-BTC with three MWCNT loadings at 35 °C and 20 mL/min. Figure 10 shows that

the CO<sub>2</sub> breakthrough time was considerably extended after the addition of MWCNTs. The CO<sub>2</sub> breakthrough time of 6%CNT-NH<sub>2</sub>-Cu-BTC was 40 min, which is twice as long as that of NH<sub>2</sub>-Cu-BTC, followed by 2%CNT-NH<sub>2</sub>-Cu-BTC and 10%CNT-NH<sub>2</sub>-Cu-BTC with CO<sub>2</sub> breakthrough times of 32 and 28 min, respectively. The CO<sub>2</sub> adsorption capacity of samples with different MWCNT loadings is depicted in Figure 11. The CO<sub>2</sub> adsorption capacity of 6%CNT-NH<sub>2</sub>-Cu-BTC reached 2.06 mmol/g, which is higher than that of the other samples. However, 10%CNT-NH<sub>2</sub>-Cu-BTC showed the lowest CO<sub>2</sub> adsorption capacity, even lower than that of 35%NH<sub>2</sub>-Cu-BTC. These results reveal that the loading of MWCNTs is beneficial for CO<sub>2</sub> adsorption, but the appropriate amount of MWCNTs should be carefully selected. This can be attributed to the generation of new mesoporous structures in the composites after MWCNT loading, which enhanced the adsorption capacity of the materials and increased the saturated CO<sub>2</sub> adsorption capacity. According to Figure 4i,j of the SEM image, it can be seen that 6% of MWCNTs doped on the surface of Cu-BTC formed a mesoporous structure. However, when the doping amount of MWCNTs reached 10%, excessive MWCNTs would agglutinate on the surface of Cu-BTC, preventing gas from entering the pore and affecting the adsorption effect. For the  $S(\text{CO}_2/\text{CH}_4)$ , after the addition of carbon nanotubes, carbon nanotubes combined with Cu-BTC to form mesoporous structures, and the adsorption of mesoporous is mainly physical adsorption. Therefore, increasing the loading capacity of carbon nanotubes will also improve the adsorption performance of CO<sub>2</sub> and CH<sub>4</sub> at the same time, resulting in a slight decrease in selectivity.

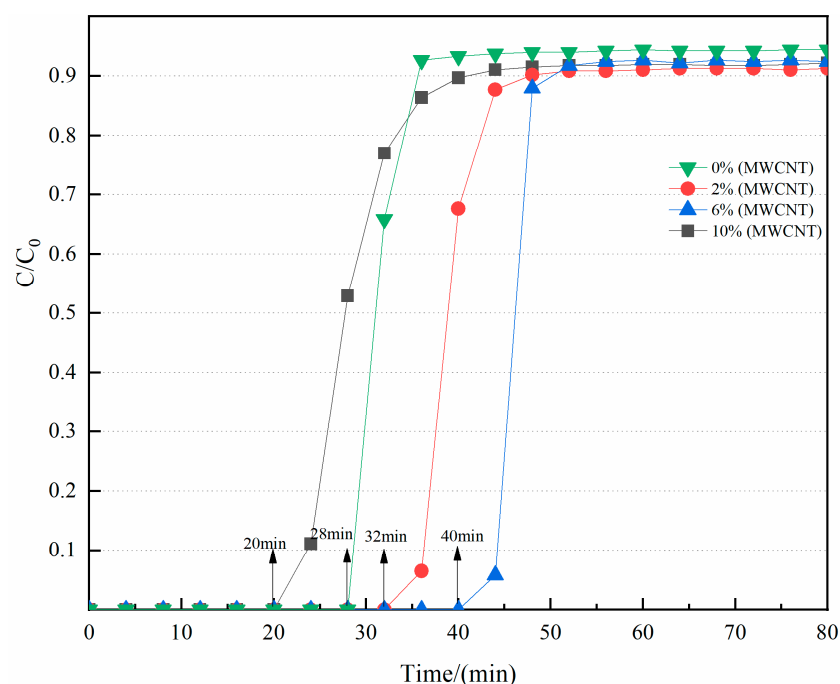


**Figure 10.** CO<sub>2</sub> breakthrough curves of CNT-NH<sub>2</sub>-Cu-BTC at different multiwalled carbon nanotube (MWCNT) loadings.

### 3.2.2. Effect of Temperature on the CO<sub>2</sub>/CH<sub>4</sub> Selective Adsorption of CNT-NH<sub>2</sub>-Cu-BTC

Adsorption experiments were conducted in the temperature range from 5 °C to 35 °C at 20 mL/min for 6%CNT-NH<sub>2</sub>-Cu-BTC. The results are depicted in Figures 12 and 13. As can be seen in Figure 12, as the temperature increased, the breakthrough time gradually extended. The CO<sub>2</sub> breakthrough time of 6%CNT-NH<sub>2</sub>-Cu-BTC was approximately 28 min when the temperature increased from 5 °C to 25 °C, and the breakthrough time increased to 40 min when the temperature reached 35 °C.

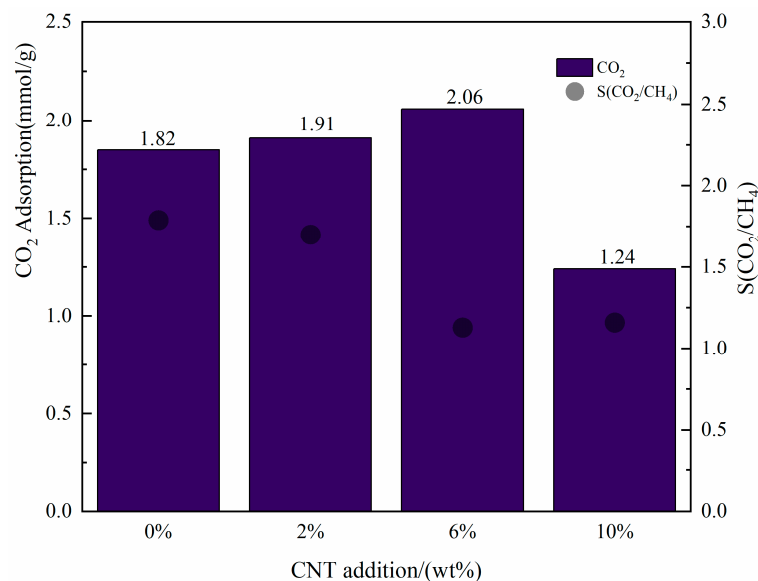


**Figure 11.** Adsorption capacity and selectivity with different MWCNT additions.

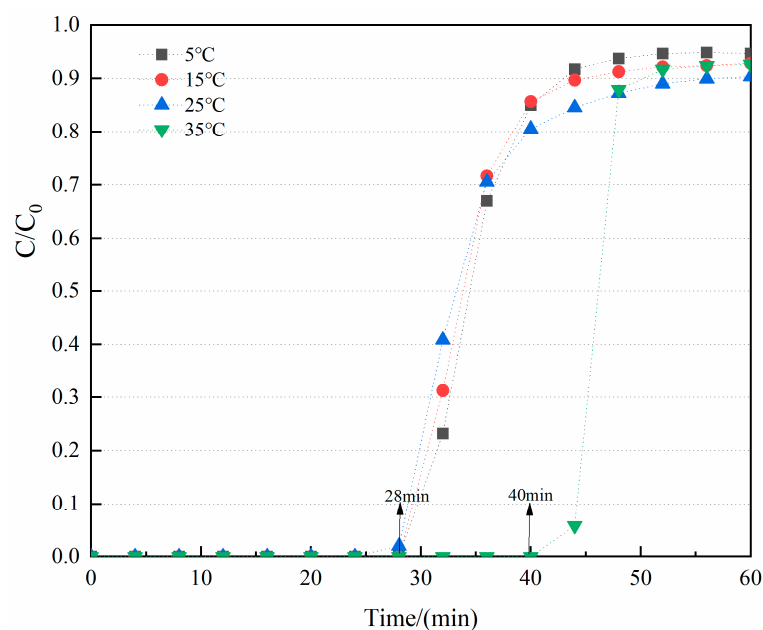


**Figure 12.** CO<sub>2</sub> breakthrough curve of 6% CNT-NH<sub>2</sub>-Cu-BTC at different temperatures.

The CO<sub>2</sub> adsorption capacity of 6% CNT-NH<sub>2</sub>-Cu-BTC increased as the temperature increased, being 1.73, 1.76, 1.82, and 2.06 mmol/g at 5 °C, 15 °C, 25 °C, and 35 °C, respectively. Generally, the adsorption capacity decreases with increasing temperature for physical adsorption. However, the opposite conclusion was observed in this study, which suggests that chemical adsorption dominates the CO<sub>2</sub> adsorption on CNT-NH<sub>2</sub>-Cu-BTC. Higher temperatures could accelerate the chemical reaction between CO<sub>2</sub> and amino groups, increasing the CO<sub>2</sub> adsorption capacity. When the temperature increases, the percentage of activated molecules increases, and the collision frequency and energy between molecules increase, which is conducive to the reaction between the active site of amine and CO<sub>2</sub>. The number of reactive molecules increases, and the breakthrough time is correspondingly extended. In our study, the experimental result showed that the reaction between amine and CO<sub>2</sub> is most intense under 35 °C.

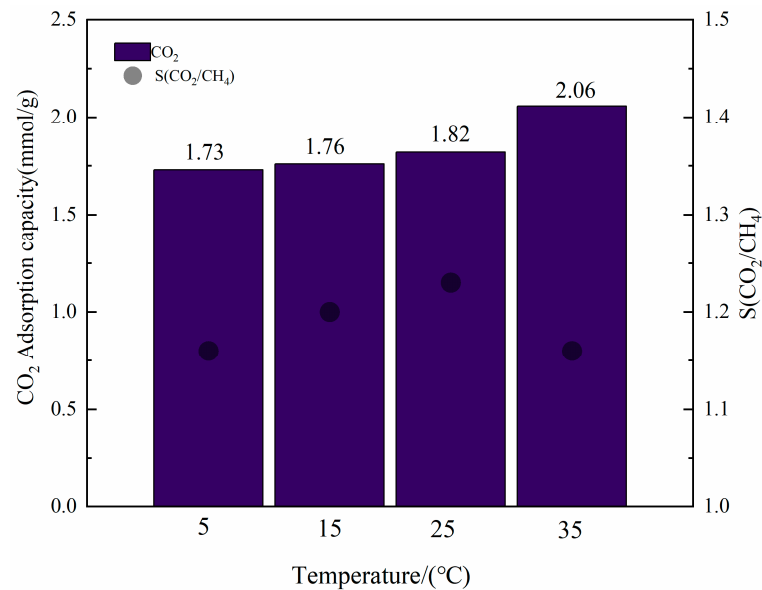


**Figure 13.** Adsorption capacity and selectivity of 6%CNT-NH<sub>2</sub>-Cu-BTC at different temperatures.

### 3.2.3. Effect of the Gas Flow Rate on the CO<sub>2</sub>/CH<sub>4</sub> Selective Adsorption of CNT-NH<sub>2</sub>-Cu-BTC

Gas flow rate is an important factor affecting the adsorption performance of adsorbents. Herein, the effect of the gas flow rate was studied by performing adsorption experiments at 15, 20, 25, and 30 mL/min and 35 °C for 6%CNT-NH<sub>2</sub>-Cu-BTC. The results are shown in Figures 14 and 15. According to Figure 14, the CO<sub>2</sub> breakthrough time first increased and then decreased with increasing gas flow rate. The longest CO<sub>2</sub> breakthrough time of 40 min was observed at 20 mL/min. The CO<sub>2</sub> breakthrough almost occurred at the start of the experiment at 30 mL/min, which indicates that the gas flow rate needs to be moderate; a larger gas flow rate is not beneficial for CO<sub>2</sub> adsorption. When the gas flow rate increased from 15 to 20 mL/min, the number of CO<sub>2</sub> molecules entering the adsorption chamber per unit time increased; that is, the inlet of CO<sub>2</sub> concentration is increased, and the kinetic energy of CO<sub>2</sub> molecules is increased, and more CO<sub>2</sub> molecules enter the pores inside the sample. In this study, the optimal gas flow rate was 20 mL/min.

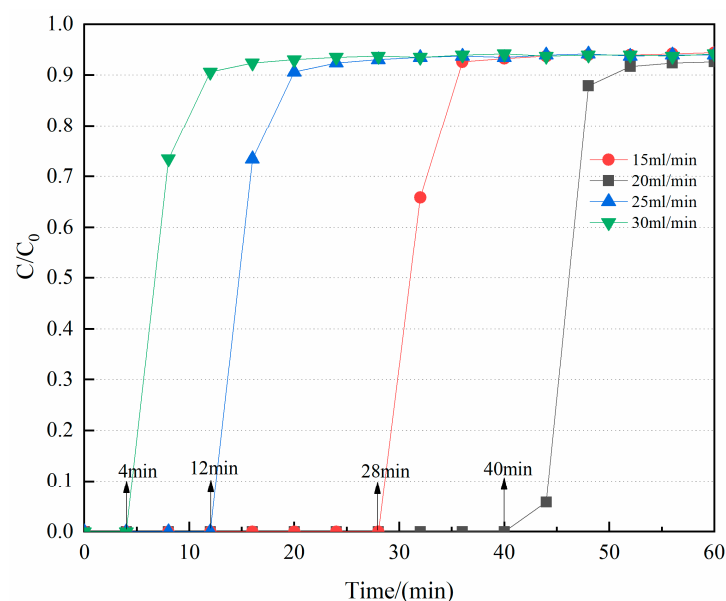


**Figure 14.** CO<sub>2</sub> breakthrough curve of 6%CNT-NH<sub>2</sub>-Cu-BTC at different flow rates.

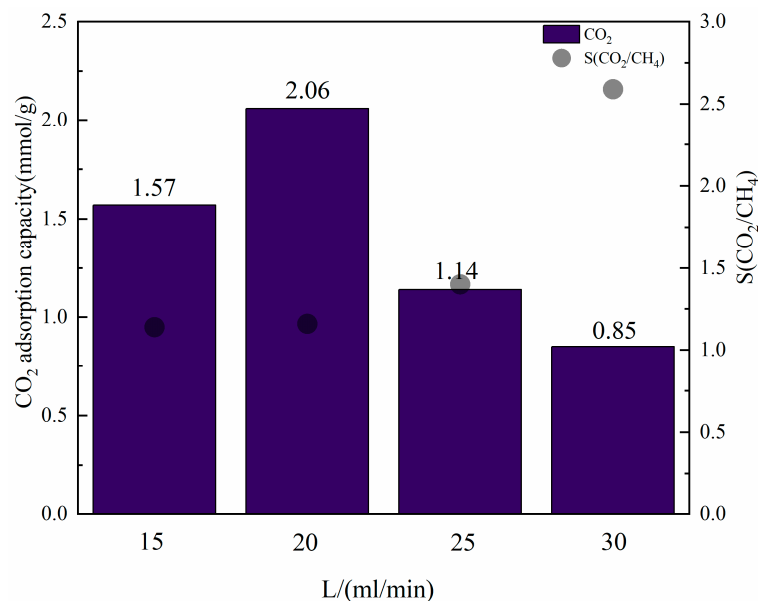


**Figure 15.** Adsorption capacity and selectivity of 6%CNT-NH<sub>2</sub>-Cu-BTC at different flow rates.

As depicted in Figure 15, with increasing gas flow rate, the adsorption capacity of CO<sub>2</sub> first increases and then decreases, which is consistent with the results of the CO<sub>2</sub> breakthrough time. According to the study of Zhang et al. [24], a lower flow rate is more conducive to the adsorption reaction. The reason may be that the contact time between the adsorbent and the adsorbed gas is sufficient at a lower gas flow rate, which prolongs the reaction time. However, in this study, when the gas flow was 20 mL/min, the adsorption capacity reached a maximum value of 2.06 mmol/g, which is higher than that at 15 mL/min. It may be that the breakthrough curves at different flow rates exhibit notable disparities, indicating that flow rate affects the adsorption rate and leads to varying times required to reach saturation. We calculated the adsorption capacity by assuming that when outlet concentration reached 95% of inlet concentration and after an adsorption time of 60 min, as shown in Figure 15, there was still a remaining 5% gas available for further absorption. Nevertheless, due to the near-saturation of the material, its adsorption rate became exceedingly slow, resulting in differences in the material's adsorption capacities at various flow rates. As shown in Figure 15, the adsorption separation of CO<sub>2</sub>/CH<sub>4</sub> was best at 30 mL/min, but the CO<sub>2</sub> adsorption capacity was the lowest. Therefore, an appropriate gas flow rate is important for the adsorption process. 6%CNT-NH<sub>2</sub>-Cu-BTC showed the best CO<sub>2</sub>/CH<sub>4</sub> selective adsorption performance at 20 mL/min.

#### 3.2.4. Water Stability of CNT-NH<sub>2</sub>-Cu-BTC

The results shown in Figure 16 demonstrate that the novel CNT-NH<sub>2</sub>-Cu-BTC composite exhibits not only enhanced CO<sub>2</sub> adsorption performance, but also improved water stability. The CO<sub>2</sub> adsorption capacity decreased after wet impregnation for all samples. The CO<sub>2</sub> adsorption capacities of Cu-BTC and NH<sub>2</sub>-Cu-BTC were 0.73 and 0.79 mmol/g, respectively, after 12 h of wet impregnation in equal volumes of deionized water, which were only 43 and 72% of those of the adsorption capacities of NH<sub>2</sub>-Cu-BTC and Cu-BTC without wet treatment, respectively. However, the CO<sub>2</sub> adsorption capacity of 6%CNT-Cu-BTC was 1.63 mmol/g after 12 h of wet impregnation, which was still 79% of the CO<sub>2</sub> adsorption capacity of untreated CNT-NH<sub>2</sub>-Cu-BTC. These results indicate that the MWCNT addition effectively improved the water stability of the material, which can be ascribed to the protection of the Cu-BTC skeleton by MWCNTs.

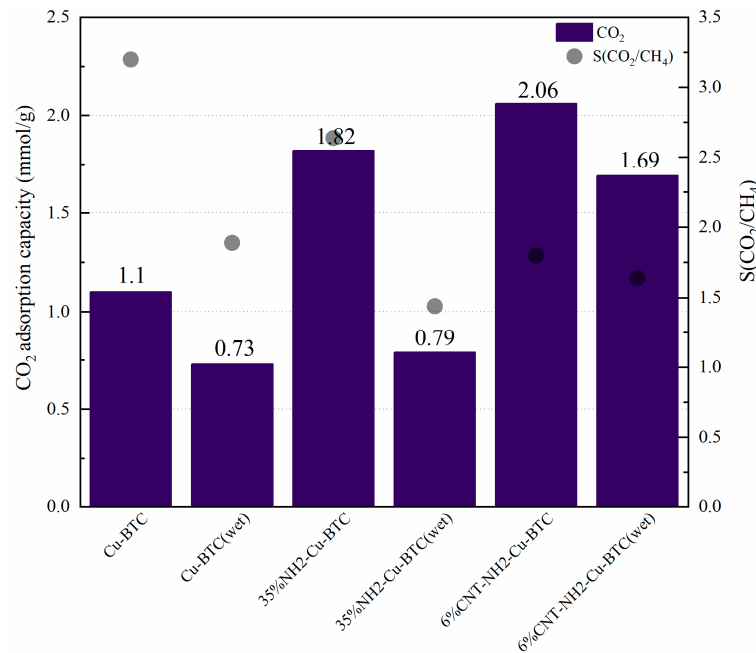


**Figure 16.** Adsorption capacity and selectivity of the samples with and without wet treatment.

### 3.2.5. Adsorption Cycles of CNT-NH<sub>2</sub>-Cu-BTC

Figure 17 shows the cyclic experiments of 6%CNT-NH<sub>2</sub>-Cu-BTC with and without wet impregnation. The CO<sub>2</sub> adsorption capacity decreased after each cycle. For 6%CNT-NH<sub>2</sub>-Cu-BTC without wet treatment, the CO<sub>2</sub> adsorption capacity was 1.23 mmol/g after the third cycle, which is 60% of the saturated adsorption capacity of the first cycle. After the fifth cycle, the CO<sub>2</sub> adsorption capacity decreased to 35% relative to the first cycle. The adsorption capacity of the samples subjected to wet treatment decreased to 0.85 mmol/g after the second cycle, which is only 50% of the initial capacity. After the fifth cycle, the adsorption capacity only reached 34% of the initial value. The reason for the poor cycles of 6%CNT-NH<sub>2</sub>-Cu-BTC material may be that when vacuum desorption is performed, the gas that is desorbed is absorbed by physical adsorption. However, if the gas adsorbed chemically fails to be released, the reaction product will occupy a part of the pore, resulting in a decrease in the cycles of the material.

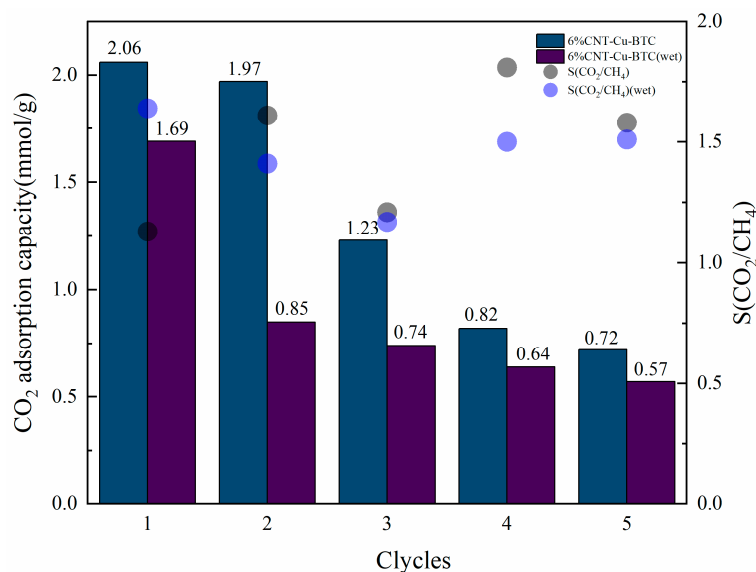


**Figure 17.** Cycle experiments.

#### 4. Conclusions

Herein, a CNT-NH<sub>2</sub>-Cu-BTC composite with enhanced CO<sub>2</sub>/CH<sub>4</sub> selective adsorption performance and water stability was prepared via hydrothermal synthesis. The XRD results showed that CNT-NH<sub>2</sub>-Cu-BTC had high crystallinity, and the modification did not destroy the parent Cu-BTC structure. The FT-IR results confirmed the successful loading of the amine functional group onto Cu-BTC. The BET and SEM results revealed that the pore structure of Cu-BTC was preserved in CNT-NH<sub>2</sub>-Cu-BTC after wet impregnation.

The CO<sub>2</sub> breakthrough experiments for Cu-BTC, NH<sub>2</sub>-Cu-BTC, and CNT-NH<sub>2</sub>-Cu-BTC showed that 6% CNT-NH<sub>2</sub>-Cu-BTC displayed the best CO<sub>2</sub> adsorption capacity and water stability, reaching a CO<sub>2</sub> adsorption capacity of 2.06 mmol/g under optimal conditions (35 °C, 20 mL/min). The introduction of MWCNTs improved the CO<sub>2</sub> adsorption capacity and water stability. The CO<sub>2</sub> adsorption capacity of 35% NH<sub>2</sub>-Cu-BTC with wet impregnation after 12 h was 1.69 mmol/g at 35 °C and 20 mL/min, which constitutes 79% of the CO<sub>2</sub> adsorption capacity of the sample without wet impregnation. The cycling experiment showed that after three cycles, 35% CNT-NH<sub>2</sub>-Cu-BTC retained 60% of the CO<sub>2</sub>-saturated adsorption capacity obtained in the first cycle.

**Author Contributions:** Conceptualization, W.J.; Data curation, Q.H. and A.Y.; Investigation, T.L.; Writing—original draft, W.J.; Writing—review and editing, D.M. and F.J. All authors have read and agreed to the published version of the manuscript.

**Funding:** This research was funded by the Basic Scientific Research Project of the Educational Department of Liaoning Province (LJKMZ20220729, JYTMS20231455), and the Liaoning Revitalization Talents Program (No. XLYC2007143).

**Data Availability Statement:** Data are contained within the article.

**Conflicts of Interest:** The authors declare no conflict of interest.

#### References

1. Wang, B.; Wang, C.; Yu, G.; Dou, K. Reflections on the development of biogas industry in Europe. *China's Energy* **2019**, *41*, 5.
2. Zheng, Y.; Zhang, Y.; Sun, B.; Zhang, B.; Zhang, S.; Jin, S.; Xiao, Z.; Chu, S.; Jing, Y.; Zhang, Z. Corrosion Behavior and Mechanical Performance of Drill Pipe Steel in a CO<sub>2</sub>/H<sub>2</sub>S-Drilling-Fluid Environment. *Processes* **2024**, *12*, 502. [\[CrossRef\]](#)
3. Hai, Q.; Jian, W.; Xie, W.; Tong, X.; Sun, Y. Research progress on adsorption of CO<sub>2</sub> by porous solid materials. *J. Liaoning P Univ.* **2022**, *42*, 30–77.
4. Granados-Pichardo, A.; Granados-Correa, F.; Sanchez-Mendieta, V.; Hernded-Mendoza, H. New CaO-based adsorbents prepared by solution combustion and high-energy ball-milling processes for CO<sub>2</sub> adsorption: Textural and structural influences. *Arab. J. Chem.* **2017**, *13*, 171–183. [\[CrossRef\]](#)
5. Wang, S.; Shen, H.; Fan, S.; Zhao, Y.; Ma, X.; Gong, J. Enhanced CO<sub>2</sub> adsorption capacity and stability using CaO-based adsorbents treated by hydration. *AIChE J.* **2013**, *59*, 3586–3593. [\[CrossRef\]](#)
6. Cláudio, R.; Soria, M.; Luís, M. Doping of hydrotalcite-based sorbents with different interlayer anions for CO<sub>2</sub> capture. *Sep. Purif. Technol.* **2020**, *235*, 1116140.
7. Khosravi, T.; Omidkhah, M.; Kaliaguine, S.; Rodrigue, D. Amine-Functionalized CuBTC/poly(ether-b-amide-6) (Pebax MH 1657) Mixed Matrix Membranes for CO<sub>2</sub>/CH<sub>4</sub> Separation. *Can. J. Chem. Eng.* **2017**, *95*, 2024–2033. [\[CrossRef\]](#)
8. Ghosh, S.; Sarathi, R.; Ramaprabhu, S. Magnesium oxide modified nitrogen-doped porous carbon composite as an efficient candidate for high pressure carbon dioxide capture and methane storage. *J. Colloid Interface Sci.* **2019**, *539*, 245–256. [\[CrossRef\]](#)
9. Guo, A.; Ban, Y.; Yang, K.; Yang, V. Metal-organic framework-based mixed matrix membranes: Synergetic effect of adsorption and diffusion for CO<sub>2</sub>/CH<sub>4</sub> separation. *J. Membr. Sci.* **2018**, *562*, 76–84. [\[CrossRef\]](#)
10. Agbaje, T.; Singh, S.; Reddy, K.S.K.; Polychronopoulou, K.; Vega, L.F.; Khaleel, M.; Wang, K.; Karanikolos, G.N. Salt-free synthesis of Cu-BTC metal-organic framework exhibiting mesoporosity and enhanced carbon dioxide adsorption. *Microporous Mesoporous Mater.* **2021**, *324*, 111265. [\[CrossRef\]](#)
11. Ahmadi, R.; Ardjmand, M.; Rashidi, A.; Rafizadeh, M. High performance novel nano adsorbents derived–Natural cellulose fibers for superior CO<sub>2</sub> adsorption and CO<sub>2</sub>/CH<sub>4</sub> separation. *Energy Sources Part A Recovery Util. Environ. Eff.* **2020**, 1–19. [\[CrossRef\]](#)
12. Mutyala, S.; Jonnalagadda, M.; Ibrahim, S.M. Effect of modification of UiO-66 for CO<sub>2</sub> adsorption and separation of CO<sub>2</sub>/CH<sub>4</sub>. *J. Mol. Struct.* **2021**, *1227*, 129506. [\[CrossRef\]](#)
13. Salehi, S.; Anbia, M. High CO<sub>2</sub> Adsorption Capacity and CO<sub>2</sub>/CH<sub>4</sub> Selectivity by Nanocomposites of MOF-199. *Energy Fuels* **2017**, *31*, 5376–5384. [\[CrossRef\]](#)
14. Ullah, S.; Shariff, A.M.; Bustam, A.; Elkhalfah, A.E.I.; Gonfa, G.; Kareem, F.A.A. The Role of Multiwall Carbon Nanotubes in Cu-BTC Metal-Organic Frameworks for CO<sub>2</sub> Adsorption. *J. Chin. Chem. Soc.* **2016**, *63*, 1022–1032. [\[CrossRef\]](#)

15. Zhang, Y.; Wibowo, H.; Zhong, L.; Horttanainen, M.; Wang, Z.; Yu, C.; Yan, M. Cu-BTC-based composite adsorbents for selective adsorption of CO<sub>2</sub> from syngas. *Sep. Purif. Technol.* **2021**, *279*, 119644. [[CrossRef](#)]
16. Eshraghi, F.; Anbia, M.; Salehi, S. Dative post synthetic methods on SBUs of MWCNT@MOFs hybrid composite and its effect on CO<sub>2</sub> uptake properties. *J. Environ. Chem. Eng.* **2017**, *5*, 4516–4523. [[CrossRef](#)]
17. Xiang, Z.; Peng, X.; Cheng, X.; Li, X.; Cao, D. CNT@Cu<sub>3</sub>(BTC)<sub>2</sub> and Metal–Organic Frameworks for Separation of CO<sub>2</sub>/CH<sub>4</sub> Mixture. *J. Phys. Chem. C* **2011**, *115*, 19864–19871. [[CrossRef](#)]
18. Liu, Q.; Gao, Y.; Zhou, Y.; Tian, N.; Liang, G.; Ma, N.; Dai, W. Highly Improved Water Resistance and Congo Red Uptake Capacity with a Zn/Cu-BTC@MC Composite Adsorbent. *J. Chem. Eng. Data* **2019**, *64*, 3323–3330. [[CrossRef](#)]
19. Li, H.; Lin, Z.; Zhou, X.; Wang, X.; Li, Y.; Wang, H.; Li, Z. Ultrafast room temperature synthesis of novel composites Imi@Cu-BTC with improved stability against moisture. *Chem. Eng. J.* **2017**, *307*, 537–543. [[CrossRef](#)]
20. Yu, L.; Liu, Q.; Dai, W.; Tian, N.; Ma, N. Efficient thiophene capture with a hydrophobic Cu-BTC-(n)Br adsorbent in the presence of moisture. *Microporous Mesoporous Mater.* **2018**, *266*, 7–13. [[CrossRef](#)]
21. Baosheng, G.; Yanyan, X.; Haoru, Z.; Sun, H.; Guo, Y.; Wang, W. High Performance Gas Separation Mixed Matrix Membrane Fabricated by Incorporation of Functionalized Submicrometer-Sized Metal–Organic Framework. *Materials* **2018**, *11*, 1421. [[CrossRef](#)]
22. Zukal, A.; Opanasenko, M.; Rubeš, M.; Nachtigall, P.; Jagiello, J. Adsorption of pentane isomers on metal-organic frameworks Cu-BTC and Fe-BTC. *Catal. Today* **2015**, *243*, 69–75. [[CrossRef](#)]
23. Saleh, T.; Gupta, V. Photo-catalyzed degradation of hazardous dye methyl orange by use of a composite catalyst consisting of multi-walled carbon nanotubes and titanium dioxide. *J. Colloid Interface Sci.* **2012**, *371*, 101–106. [[CrossRef](#)]
24. Zhang, G.; Zhao, P.; Hao, L.; Xu, Y. Amine-modified SBA-15(P): A promising adsorbent for CO<sub>2</sub> capture. *J. CO<sub>2</sub> Util.* **2018**, *24*, 22–33. [[CrossRef](#)]

**Disclaimer/Publisher’s Note:** The statements, opinions and data contained in all publications are solely those of the individual author(s) and contributor(s) and not of MDPI and/or the editor(s). MDPI and/or the editor(s) disclaim responsibility for any injury to people or property resulting from any ideas, methods, instructions or products referred to in the content.